Gain-scheduled controller for the suppression of convection at high Rayleigh number

A. C. Or and J. L. Speyer
Department of Mechanical and Aerospace Engineering, University of California, Los Angeles, California 90095-1597, USA
(Received 14 June 2004; revised manuscript received 28 October 2004; published 4 April 2005)

Recent studies in the feedback control of Rayleigh-Bénard convection indicate that one can sustain the no-motion state at a moderate supercritical Rayleigh number (Ra) using only proportional compensation. However, stabilization occurs at a much higher Rayleigh number using linear-quadratic-Gaussian (LQG) control synthesis. The restriction is that the convection model is linear. In this paper, we show that a comparable degree of stabilization is achievable for a fully nonlinear convection state. The process is demonstrated in two stages using a fully nonlinear, 3D Boussinseq model, compensated by a reduced-order LOQ controller and a gain-schedule table. In the first stage a fully-developed convective state is suppressed through the control action at a moderate supercritical Ra. After the residual convection decays to a sufficiently small amplitude, in the second stage, we increase the Ra by a large step and switch the compensator gains using the gain-schedule table. During this change the control action is in place. Our nonlinear simulation results suggest that the nonlinear system can be stabilized to the limit predicted by the linear analysis. The simulation shows that the large Ra jump induces a large transient temperature in the conductive component, which appears to have very small impact on the stabilization.

DOI: 10.1103/PhysRevE.71.046302 PACS number(s): 47.20.Bp

I. INTRODUCTION

Considerable interest has been demonstrated in the suppression of convection using the optimal control methods [1]. A glimpse at some important results can be found in [2] using the Boussinesq model for Rayleigh-Bénard convection (RBC). The suppression of the onset of RBC by feedback control was investigated through analyses, experiments, and numerical simulations by a number of authors. The results were published in [3–11]. Potential industrial applications of the technique occur in several areas, such as material processing, moulding, and crystal growth. The outlook is encouraging.

The proportional feedback control used by Tang and Bau [3,7,8] and by Howle [4–6,11] offers a simple, intuitive way to control the system. The mechanism of suppression corresponds to the spatial stabilization of the unstable perturbation temperature field by the temperature control. From a control analysis point of view, a proportional control law is often considered insufficient. To account for the complete spatial-temporal dynamics, linear-quadratic-Gaussian (LQG) synthesis offers much better performance, as demonstrated in [1,9,10]. LQG synthesis also provides a systematic and optimal methodology to design a high-order robust compensator that guarantees a certain level of relative stability margins. Furthermore, with LQG synthesis there is an existing body of modern control theory literature to aid in the issues of controller implementation, systematic order reduction, and gain scheduling.

We published two studies in applying the LQG synthesis for controlling RBC. The first study is a closed-loop linear stability analysis [9], in which detailed stability boundary curves were computed. The no-motion state can be stabilized up to 14.5 times the critical Rayleigh number Ra_c for the case of moderate Prandtl number (Pr=7.0). Beyond this limit the LQG controller allows islands of instability to form below Ra=14.5 times of Ra_c.

The linear stability results is very restricted because in real applications convection has finite amplitudes. In the second study, a three-dimensional nonlinear plant model [10] was developed using the pseudo-spectral method. Using LQG synthesis of [9], we demonstrated that a fully nonlinear initial steady convection state at about 6 times the critical Rayleigh number can be damped out by control action. The no-motion state is sustained.

In all the studies [1–10], the measurements and control actions were assumed to be spatially continuous. No sensor or actuator dynamics were included. In a more recent study by Howle [11], it was demonstrated that the finite wall thickness in the boundaries adds additional actuator dynamics and alters the onset mode of instability. Here, this added latency has not been included. This area is of interest for future investigations.

In this study our goal is to demonstrate that a fully nonlinear convection state can be suppressed, and the convection-suppressed, no-motion state can be raised to a Ra value comparable to the stability limit dictated by the linear analysis. A two-stage gain-schedule approach is considered here. Furthermore, a reduced-order LQG controller has been developed for this task.

II. 3D NONLINEAR PLANT MODEL

Consider an infinite layer of Boussinesq fluid (see the schematic of Fig. 1). The upper wall is maintained at temperature T_2^* and the lower wall temperature at $T_1^*+\beta\Delta T^*+\theta_c^*$, where $T_1^*>T_2^*$; the flag β is set to zero prior to the step jump in Ra and equal to one after the jump; ΔT^* is the step increase in lower-wall temperature corresponding to the Ra step. These are the conductive components of the temperature. To suppress convection, a temperature control $\theta_c^*(x,y)$ is generated on the actuator plane assumed to coincide with the lower wall. This is a perturbation temperature.

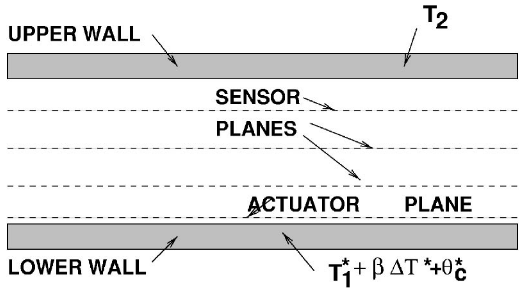

FIG. 1. Schematic of a section of the 3D fluid layer.

There are three embedded sensor planes in the layer, which measure the interior field temperatures at three different levels, $z_s^{(i)}$ $(i=1,2,3)$. The perturbation sensor temperatures from the conductive component are denoted as $\theta_s^*(x,y,z_s^{(i)})$.

Due to the step increase in Ra, a transient temperature is generated in the conductive component of the total temperature after the step increase. The heat equations for the static conductive temperature and transient conductive temperature, and for the perturbation temperature due to convection are derived from first principles in the Appendix. In the presence of convection, the total temperature is decomposed into the conductive and convective components. The conductive temperature has a transient component as well. The nominal conductive temperature is the static component. The conductive temperature field is stable. The convective temperature has a nominal of zero. The control loop is designed to drive this perturbation component to zero. In the nondimensional mathematical form, the quantities d, d^2/κ, κ/d, κ/d^2, $\rho(\kappa/d)^2$, and $(T_1^*-T_2^*)$ (before the Ra step) and $(T_1^*+\Delta T^*-T_2^*)$ (after the Ra step), are used as the scales of length, time, velocity, vorticity, pressure, and temperature, where d is the layer thickness, κ and ρ are the mean thermal diffusivity and density of the fluid.

The governing nondimensional Oberbeck-Boussinesq equations are

$$\mathrm{Pr}^{-1}\partial_t \mathbf{v} = \mathrm{Pr}^{-1}\mathbf{v}\times\boldsymbol{\omega} + \mathbf{k}\mathrm{Ra}\,\theta - \nabla\pi_e + \nabla^2\mathbf{v}, \tag{1}$$

$$\partial_t\theta = -\mathbf{v}\cdot\nabla\theta + w(1-\partial_z\tilde{\Theta}) + \nabla^2\theta, \tag{2}$$

$$\partial_t\tilde{\Theta} = \partial_{zz}^2\tilde{\Theta}, \tag{3}$$

$$\nabla\cdot\mathbf{v} = 0, \tag{4}$$

where $\mathbf{v}=(u,v,w)$ is the velocity vector field, $\boldsymbol{\omega}=\nabla\times\mathbf{v}$ is the vorticity, $\pi_e=\pi+\mathbf{v}\cdot\mathbf{v}/2$ is the effective pressure head, $\tilde{\Theta}(z,t)$ is the transient component in the conductive temperature, θ is the perturbation temperature due to convection, and $\mathbf{k}$ is unit vector in the z direction. The two external parameters are the Rayleigh number and the Prandtl number, respectively, defined by $\mathrm{Ra}=\alpha g\Delta T^* d^3/\nu\kappa$ and $\mathrm{Pr}=\nu/\kappa$ where α is the coefficient of thermal expansion and ν is the mean kinematic viscosity. The continuity equation (4) is for an incompressible flow.

The upper and lower wall velocity field conditions are nonpermeable and nonslip,

$$\mathbf{v}(x,y,0,t)=\mathbf{0}, \quad \mathbf{v}(x,y,1,t)=\mathbf{0}. \tag{5}$$

The upper and lower wall transient conductive temperatures have a zero initial condition before the step jump, since the layer is in a steady state heat conduction prior to the step increase of Ra. After the step increase, at $t=t^+$, the initial condition for $\tilde{\Theta}$ is given by

$$\tilde{\Theta}(z,t^+) = -\frac{\Delta T^*(1-z)}{(T_1^*+\Delta T^*-T_2^*)}. \tag{6}$$

The boundary conditions are homogeneous,

$$\tilde{\Theta}(0,t)=0, \quad \tilde{\Theta}(1,t)=0. \tag{7}$$

The upper-wall boundary condition for the perturbation temperature is homogeneous. The lower-wall boundary condition for the perturbation temperature includes the temperature control $\theta_c(x,y,t)$, which is generated by the actuator action. The upper and lower thermal boundary conditions for the perturbation temperature are

$$\theta(x,y,1,t)=0, \quad \theta(x,y,0,t)=\theta_c(x,y,t). \tag{8}$$

The temperature field is measured on the three embedded sensor planes at the levels $z=z_s$ $(s=1,2,3)$. Since the conductive temperature field in the layer can be determined independently, we can subtract it from the total to obtain the perturbation temperature measurements. The perturbation sensor temperature measurements are

$$\theta_s(x,y,t)=\theta(x,y,z_s,t), \quad s=1,2,3. \tag{9}$$

In the numerical scheme the three-dimensional (3D) dependent variables u, v, w, p, and θ are expressed by the following finite triple sums:

$$\begin{bmatrix} u \\ v \\ w \\ p \\ \theta \end{bmatrix}(x,y,z,t) = \mathrm{Re}\left\{\sum_{n=0}^{N}\sum_{k=0}^{K}\sum_{m=-M+1}^{M}\begin{bmatrix} u_{kmn} \\ v_{kmn} \\ w_{kmn} \\ p_{kmn} \\ \theta_{kmn} \end{bmatrix}(t)T_n \times(z)e^{i(k\alpha_x x+m\alpha_y y)}\right\}. \tag{10}$$

where Re denotes the real part of the sum; α_x and α_y are the fundamental wave numbers in the x and y directions, respectively. The two fundamental wave numbers are prescribed. Here, the number of total coefficients can be reduced to half by only including the coefficients for $k\geqslant 0$, because all the dependent variables are real (see detailed description in [10]). The functions $T_n(z)$ $(n=0,1,\ldots)$ denote the Chebyshev polynomials. A linear coordinate transformation is used to convert the Chebyshev function domain from the function domain $-1\leqslant z<1$ to our physical domain $0\leqslant z<1$. The perturbation temperature control θ_c and measurement temperatures θ_s $(s=1,2,3)$, are planar. They are expanded as double sums,

$$\begin{bmatrix}\theta_s(z_1,t)\\ \theta_s(z_2,t)\\ \theta_s(z_3,t)\\ \theta_c(0,t)\end{bmatrix}(x,y,t) = \mathrm{Re}\left\{\sum_{k=0}^{K}\sum_{m=-M+1}^{M}\begin{bmatrix}\theta_{km,s}(z_1,t)\\ \theta_{km,s}(z_2,t)\\ \theta_{km,s}(z_3,t)\\ \theta_{km,c}(0,t)\end{bmatrix} \times e^{i(k\alpha_x x+m\alpha_y y)}\right\}. \tag{11}$$

III. THE REDUCED-ORDER LQG COMPENSATOR

The LQG synthesis method was discussed in detail in [9]. In the study, the LQG compensator used is full ordered, that is, the compensator has the same order as the 3D nonlinear convection model. The controller was demonstrated to be effective in removing the convection state, reverting the layer back to its no-motion state for $\mathrm{Ra}=10^4$, about 5.8 times the critical value. In this paper, the full-order compensator is replaced by a reduced-order compensator. A methodology for increasing Ra was developed without destabilizing the controlled state. This is a gain scheduling approach.

To design a reduced-order compensator, the linear Boussinesq equations are expressed in a state-space form for each Fourier-decomposed mode [corresponding to wave numbers $(k\alpha_x, m\alpha_y)$]. The state-space system includes the corresponding measurement (sensor) equations and the control (actuator) equations. We remark that these are the linearized equations about the no-motion state, not about the nonlinear convective state. For the simplicity of notations, the indices for the wave numbers are omitted. It is clear that there is a distinct set of state-space equations for each pair of wave numbers for each Fourier mode for each Rayleigh number. The state space equation is expressed as

$$\dot{\mathbf{x}} = \mathbf{A}\mathbf{x} + \mathbf{B}\mathbf{u}, \tag{12}$$

where the state vector $\mathbf{x}$ consists of the Chebyshev coefficients for the velocity and the temperature perturbations for wave number pair $(k\alpha_x, m\alpha_y)$; u is the Fourier coefficient of the temperature control according to Eq. (11). The sets of state space equations (12) corresponding to different wave-number pairs are decoupled in a linear sense.

From Eqs. (11) and (10), we denote the measurement temperature Fourier coefficients by the three-row vector $\mathbf{z}$; $\mathbf{z}$ consists of measurement on 3 planes z_1, z_2, z_3, which can be expressed in terms of the state vector by the matrix equation

$$\mathbf{z} = \mathbf{C}\mathbf{x}. \tag{13}$$

We show a block diagram for the control loop between the compensator and the plant model by a schematic in Fig. 2. The LQG compensator consists of a Kalman filter and an optimal regulator. The fixed-gain Kalman filter equation and the optimal regulator equation are, respectively,

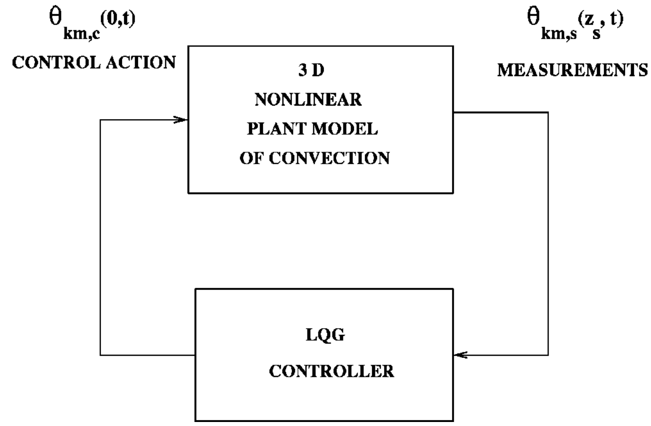

FIG. 2. The control loop diagram.

$$\dot{\hat{\mathbf{x}}} = \mathbf{A}\hat{\mathbf{x}} + \mathbf{B}\mathbf{u} + \mathbf{K}_f(\mathbf{z} - \hat{\mathbf{z}}), \quad u = -\mathbf{K}_c\hat{\mathbf{x}}, \tag{14}$$

where vector $\hat{\mathbf{x}}$ consists of the state estimates. The following measurement equation relates the estimates of measurements to the estimates of the true states,

$$\hat{\mathbf{z}} = \mathbf{C}\hat{\mathbf{x}}. \tag{15}$$

The steady-state Kálman gain vector $\mathbf{K}_f$ and the regulator gain vector $\mathbf{K}_c$ are determined from two steady-state algebraic Riccati equations (AREs) [1,9].

To determine the controller gain $\mathbf{K}_c$, the states $\mathbf{x}$ and control u are quadratically penalized in an integral cost criterion. The associated weightings are used in the controller AREs. To determine the filter gain $\mathbf{K}_f$, we assumed that Gaussian noises are added to the dynamics and the measurements. The power spectral densities are used as the design parameters in the AREs to form the gains. The LQG compensator at each Ra number consists of $2(K+1)M$ sets of state space matrices $(\mathbf{A},\mathbf{B},\mathbf{C},\mathbf{D})$ (where $\mathbf{D}=\mathbf{0}$), and the same number of sets of gains $\mathbf{K}_f, \mathbf{K}_c$. There is no cross coupling between the sets of equations. Each set is designed to compensate for a Fourier mode corresponding to a wave number pair. In the full-order controller formulation, the dimension of $\mathbf{A}$ ranges from 64 to 128, K and M range from 32 to 64. The compensator becomes very large.

We have considered two different approaches to design the order-reduced compensator. The first approach is to seek a balance between the input and output relationships of the plant model. The second approach is to seek a balance between the input and output relationships of the compensator. The state space system is first transformed to a Schur canonical form and then ordered block by block in a balanced realization scheme (grammian-based). The reduced-order compensator is then constructed based on the reduced-order dynamics and their input-output relationships.

The first approach appeared to be quite effective when applied to controlling the laminar boundary layer transition [12]. However, when applied to Rayleigh-Bénard convection, the reduced-order compensator is not as robust as it should be. Some preliminary simulation results indicate that an order reduction by a factor of 2 is possible. Further reduction makes the closed-loop response unstable.

The first approach is not robust. Our ultimate goal is to use a reduced-order compensator to control a full-order nonlinear plant model. The reason that we perform a balance realization on the linearized plant model, and then truncate the plant model, is because we want to use the reduced-order linear plant model to design the reduced-order compensator. In the second approach, we do not truncate the plant model. We first design a full-order compensator for the full-order plant model, just as in [9]. Then, we seek to perform a balance realization on the compensator instead, and then truncate compensator model. By doing that we have to compute the full-order Kalman gains $\mathbf{K}_f$ and full-order regulator gain $\mathbf{K}_c$ based on the full-order plant model with state space ($\mathbf{A}$, $\mathbf{B}$, and $\mathbf{C}$). Then, we perform a balance realization on the compensator input and output. The compensator inputs the measurement vector $\mathbf{z}$ and outputs the control vector $\mathbf{u}$.

From Eq. (14), we obtain the following state space equations for the full-order compensator,

$$\dot{\hat{\mathbf{x}}} = \mathbf{A}_c\hat{\mathbf{x}} + \mathbf{B}_c\mathbf{z},$$
$$\mathbf{u} = \mathbf{C}_c\hat{\mathbf{x}} + \mathbf{D}_c\mathbf{z}. \tag{16}$$

The subscript "c" denotes the compensator, where the state space matrices are given by

$$\mathbf{A}_c = \mathbf{A} - \mathbf{B}\mathbf{K}_c - \mathbf{K}_f\mathbf{C} + \mathbf{K}_f\mathbf{D}\mathbf{K}_c,$$
$$\mathbf{B}_c = \mathbf{K}_f, \quad \mathbf{C}_c = -\mathbf{K}_c, \quad \mathbf{D}_c = \mathbf{0}, \tag{17}$$

where $\mathbf{D}_c=\mathbf{0}$. To reiterate, in the first approach the balance realization is performed on $(\mathbf{A},\mathbf{B},\mathbf{C})$. In the second approach, the balance realization is performed on $(\mathbf{A}_c,\mathbf{B}_c,\mathbf{C}_c,\mathbf{D}_c)$ instead. It is worth noting that the dynamics of $\mathbf{A}_c$ can be distinctively different from those of $\mathbf{A}$. The compensator dynamics now depends on the gain vectors as the input and output matrices.

A grammian-based balance realization is just one way to perform the balancing. A typical grammian-based routine is by solving the Lyapunov-type equations using the polynomial methods. The polynomial routines are not effective for large matrices. Here, we consider an approximate method. First, we apply a similarity transformation $\mathbf{x}=\mathbf{P}\mathbf{x}_1$, in which the transformation $\mathbf{P}$ diagonalizes $\mathbf{A}_c$. This transformation converts $(\mathbf{A}_c,\mathbf{B}_c,\mathbf{C}_c,\mathbf{D}_c)$ into $(\mathbf{A}_{c1},\mathbf{B}_{c1},\mathbf{C}_{c1},\mathbf{D}_{c1})$. If there are nondistinct eigenmodes, then we have to use the Schur canonical transformation instead. The transformation is

$$\mathbf{A}_{c1} = \mathbf{P}^{-1}\mathbf{A}_c\mathbf{P}, \quad \mathbf{B}_{c1} = \mathbf{P}^{-1}\mathbf{B}_c,$$
$$\mathbf{C}_{c1} = \mathbf{C}_c\mathbf{P}, \quad \mathbf{D}_{c1} = \mathbf{D}_c, \tag{18}$$

where $\mathbf{A}_{c1}$ is now in a diagonal form. We denote the diagonal entries of this matrix by λ_i $(i=1,2,\ldots,N)$. We allow the diagonal entries to be expressed in complex conjugate pairs.

Second, we define a score parameter for each compensator mode, denoted as σ_i $(i=1,2,\ldots,N)$, where

$$\sigma_i = |\mathbf{b}_i||\mathbf{c}_i|/|\lambda_i|, \quad i = 1,2,\ldots,N, \tag{19}$$

$\mathbf{b}_i$ is the ith row of $\mathbf{B}_{c1}$ and $\mathbf{c}_i$ is the ith column of $\mathbf{C}_{c1}$. Then we perform a reordering, in which the eigenmodes in $(\mathbf{A}_{c1},\mathbf{B}_{c1},\mathbf{C}_{c1},\mathbf{D}_{c1})$ are ranked according to the magnitude of the score parameter. The modes are arranged in the order of importance. The unimportant modes at the end will be truncated. A truncated, reduced-order set is denoted by $(\mathbf{A}_{c2r},\mathbf{B}_{c2r},\mathbf{C}_{c2r},\mathbf{D}_{c2r})$, with the state vector $\mathbf{x}_{1r}$ (subscript "r" stands for reduced-order set).

The reduced-order compensator is described by

$$\dot{\hat{\mathbf{x}}}_{1r} = \mathbf{A}_{c2r}\hat{\mathbf{x}}_{1r} + \mathbf{B}_{c2r}\mathbf{z},$$
$$\mathbf{u} = \mathbf{C}_{c2r}\hat{\mathbf{x}}_{1r} + \mathbf{D}_{c2r}\mathbf{z}. \tag{20}$$

IV. RESULTS

The preferred convection pattern is steady, two-dimensional (2D) finite-amplitude rolls. We start at $\mathrm{Ra}=10^4$ and use the steady convection rolls as the initial condition. Although the preferred wavenumber of the rolls is about 3.1, in our simulation, the fundamental wavenumbers are chosen to be at $\alpha_x=1.0$ and $\alpha_y=1.0$. So, the steady rolls occur as the longitudinal rolls (parallel to y axis) in the second Fourier harmonic. Three-dimensional zero-mean Gaussian noises (zero mean, standard deviation equal to 10^{-6}) are added to each coefficient in the initial fields. This ensures that if 3D instabilities occur, there exists perturbations for them to grow. The full-order nonlinear plant model has a resolution of 2×128 Chebyshev modes in the vertical direction (for both vertical velocity and temperature) and 32×32 Fourier modes in the horizontal direction. Note that the horizontal velocity is obtainable from the vertical velocity through the continuity equation. In the reduced-order compensator, only eight Chebyshev modes (complex) are retained. The same number of Fourier modes is used in the horizontal direction. The analysis shows that 8 Chebyshev modes is the minimum for effective control.

A. Closed-loop simulation prior to the Ra increase

The first-stage of simulation is performed using the first set of gains in the gain-schedule table. The simulation is performed until the residual convection is sufficiently small. The simulation shows that a time period of 0.4 unit is sufficient for the purpose. With a time step of $\Delta t=0.0004$, we sample the output every five time steps. The maximum temperature control recorded occurs right at the start, i.e., at $t=0.004$. The temperature control produces a sharp peak in the transient phase of roughly 0.15 time unit wide. This peak has a maximum roughly of 1.3 times the conductive temperature difference imposed across the upper and lower walls, that is, ΔT. This $1.3\Delta T$ may be considered high for experimental implementations. It all depends on the saturation limit of the actuator. If saturation occurs, then we have to reduce the Ra value of the initial condition.

The question of using a linear controller to control a nonlinear system needs an explanation. In fact, the linear system consists of only the one Fourier mode. Therefore, in the linear sense the controller is a single-mode controller [3–6,9]. The nonlinear system consists of an infinite number of Fourier modes, all except one are generated by the nonlinear

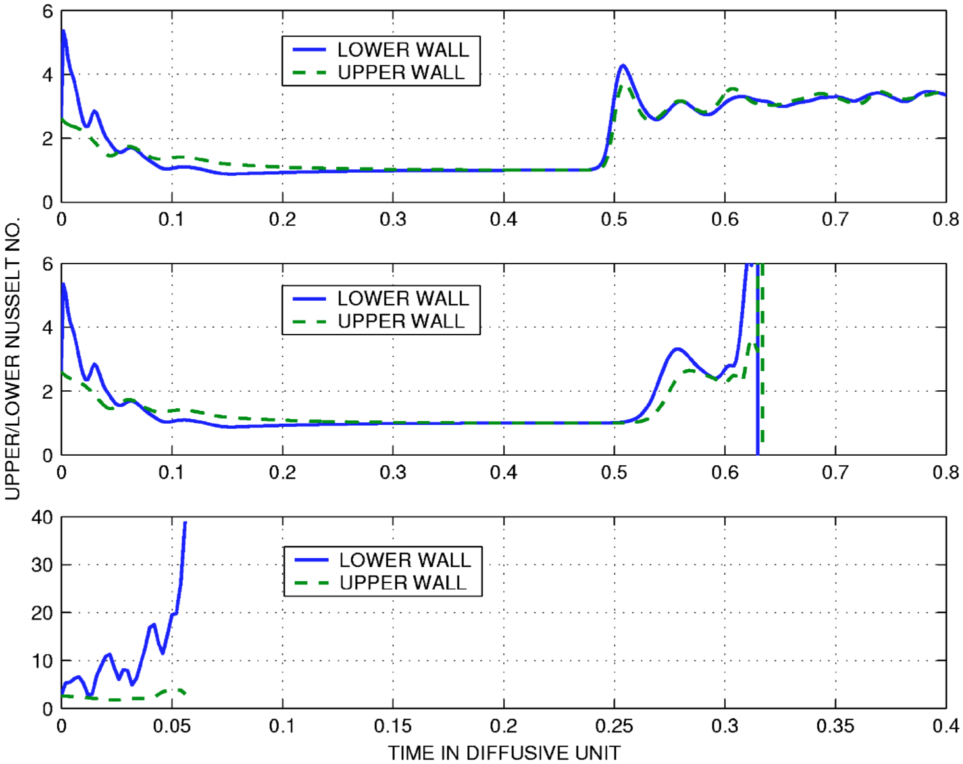

FIG. 3. Closed-loop responses on three test cases.

terms. Other than the Fourier modes, there always exists a mean temperature field as well. The linear controller controls each Fourier mode, as well as the mean field, individually. Even though each mode is treated as linear by the controller, a linear controller has been proven effective. In fact, it should be effective, as long as the higher-order terms in the amplitude expansion corresponding to a particular Fourier mode is either stabilizing or insignificant. Therefore, the temperature control containing a horizontal mean component is obvious but was not explicitly mentioned in [9]. This mean component is reasonably large too. At the peak of the temperature control, this component is about $-0.35\Delta T$. It tends to zero as convection is suppressed.

The Nusselt number Nu is defined as the ratio of the total (convective and conductive) to the purely conductive heat transfer. This parameter is a measure of the degree of convective activities. In the closed-loop response, it is also a measure of the effectiveness of the controller. In Figs. 3 and 4, the Nusselt numbers at the lower wall (Nu_1, solid line) and upper wall (Nu_2, dashed line) are plotted as functions of time. When $Nu_1 = Nu_2 = 1.0$, the layer is purely conductive, i.e., there is no convection motions. However, the conductive state can be transient. When $Nu_1 > Nu_2$, relative to conduction, net heat is pumped into the layer via the lower wall. This situation is observed at the beginning of the closed-loop simulation (for time less than 0.07) in every case, indicating that the controller starts by pumping net heat into the layer. When $Nu_2 > Nu_1$, net heat (relative to conduction) is extracted from the layer. It is possible for the transience to cause $Nu_1 < 1.0$ as convection is damping out, as seen in the conductive case (see Fig. 4). At small convection amplitude (as the Nusselt number approaches 1.0), the nominal simulation (see Fig. 4) shows that the upper-wall Nusselt number has value greater than 1.0 and the lower-wall Nusselt number has value less than 1.0. This linear behavior shows that the controller action is to extract net heat (relative to conduction) from the layer, thereby reducing the convection energy.

B. Gain scheduling, Ra stepping and the transient response of the conductive temperature

The gain scheduling is a means to allow the filter and control gains to vary during the closed-loop simulation. Typically, a gain table is constructed. The Ra range is divided into intervals. Each interval corresponds to a new set of gains. In the simulation, as Ra is increased through the intervals in time, the gains are switched to preserve the control performance. For implementation, it is more convenient to increase Ra by steps. A step jump causes transience in the conductive temperature component. This may in turn cause perturbations in the convective field. In this study, we consider only a two-interval gain-table, since each set of gains is extremely large even for the reduced-order controller [32×32 sets of reduced-order state space $(\mathbf{A}, \mathbf{B}, \mathbf{C}, \mathbf{D})$]. We use a large step increase in Ra to assess the performance. The key, however, is not to destabilize the closed-loop system.

In the simulation we consider a step increase of Ra from 10^4 to 2×10^4. The simulation following the step at $t = t^+ = 0.4$ unit continues for 0.4 time unit. The total simulation time is 0.8 unit.

Before performing the nominal simulation, we consider three test cases (shown in the three panels of Fig. 3). The purpose of the tests is for sanity checks and also for a better understanding of the closed-loop response in general. In the test case 1 (see Fig. 3, upper panel), the control action is disconnected right after the Ra step increase at $t = t^+ = 0.4$.

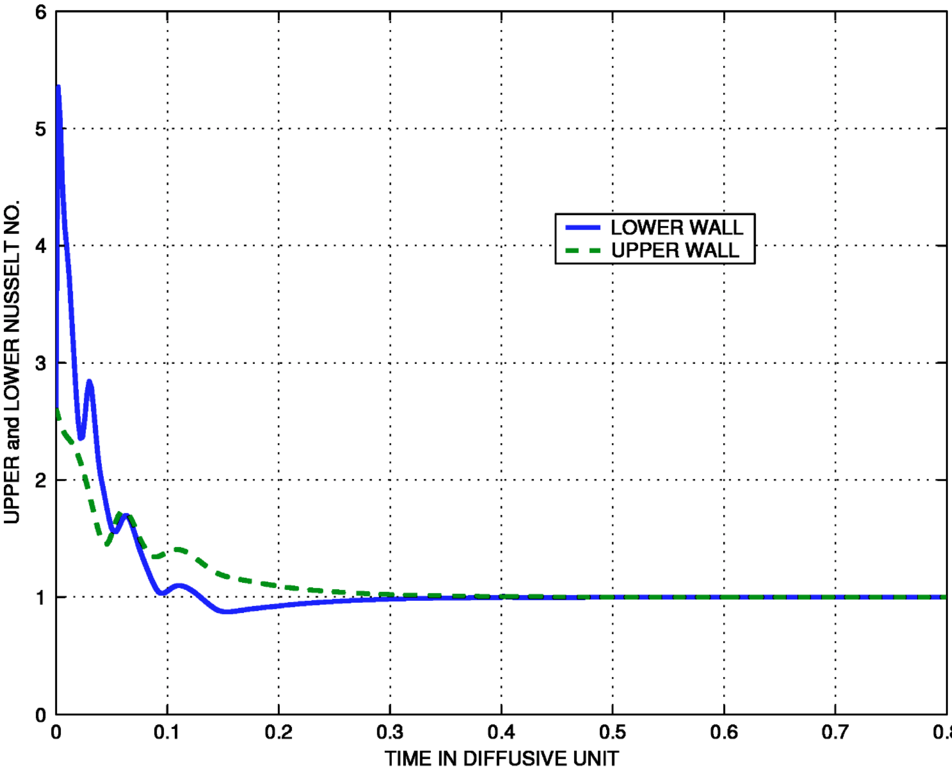

FIG. 4. Closed-loop upper and lower Nusselt numbers.

The remaining simulation has no feedback control. The key observation is that it takes a long duration for convection to build up again. Eventually, the layer has reverted the suppressed state to full-blown, finite-amplitude steady-state of convection. The behavior is indicated by the Nu_2 (dashed line) and Nu_1 (solid line). The curves converge to its steady state value at about 3.0.

In the test case 2 we maintain a closed loop throughout the simulation. However, we do not switch the gains at the step increase of Ra. Figure 3 (the middle panel) shows that the original set of gains is ineffective to maintain the no-motion state. Even worse than the test case 1, the closed loop response displays finite-time divergence. In this case, the system does not settle to a steady state. It blows up.

A set of gains designed at a higher Ra is not necessarily effective to control the layer at a lower Ra. In the test case 3, we use the second set of gains (designed at $\mathrm{Ra}=2\times 10^4$) to control convection before the Ra step increase (the steady state at $\mathrm{Ra}=10^4$). The result (Fig. 3, lower panel) shows that the closed loop response is divergent.

Finally, we turn to the nominal case of the two Ra-step simulation. In this case, we use the gains according to the gain table. show the closed-Loop response in Fig. 4. At $t=t^+=0.4$, we see a very small kink in the solid curve corresponding to Nu_1, due to the transient conductive temperature. The important observation is that the transient conductive temperature has very little impact on the residual convection.

Unfortunately, the Nusselt number plots do not show the detailed transience of the residual convection on the scale used to plot Fig. 4. It is of interest to show the control temperature θ_c in the closed-loop response. Referring to Eq. (11), we define the plotted quantity $\|\theta_c\|$ as

$$\|\theta_c\| = \left\{ \sum_{k=0}^{K} \sum_{m=-M+1}^{M} \theta_{km,c}(0,t)\overline{\theta_{km,c}(0,t)} \right\}^{1/2}. \qquad (21)$$

This measure is plotted in a semilogarithm scale (see Fig. 5). The regions of steep slopes indicate locations where a cross over zero has occurred. The maximum of the mean temperature control occurs at the beginning of the simulation. The maximum value is 1.27. Near $t=0.4$, a distinct jump is observed. This is due to the conductive temperature transience caused by the step increase in Ra. The dominant coefficient (greater than 96% of the norm, corresponds to the coefficient for $k=3$ and $m=0$, as expected. This coefficient represents the longitudinal convection rolls at a wave number 3.0, as prescribed. All the coefficients for $m\neq 0$ vanish. The results suggest that a large step increase of Ra is benign. The large transient conductive temperature does not destabilize the closed-loop system.

In Fig. 6, we plot the transient conductive temperature, $\tilde{\Theta}(z,t)=\Theta(z,t)-\Theta_{ss}(z)$ at several time points, at $t=0.4$, 0.48, 0.56, and 0.72. The quantity converges to zero fairly rapidly.

V. CONCLUSIONS

In this study two important steps have been advanced using a robust control synthesis for the problem of suppression of convection: (i) a reduced-order compensator and (ii) a simulation based on a two-step gain-schedule table. For compensator order reduction, the simulation results show that eight Chebyshev modes is the minimum for an effective performance. In stepping the Ra by a large increment using the gain schedule table, an interesting observation is that a large

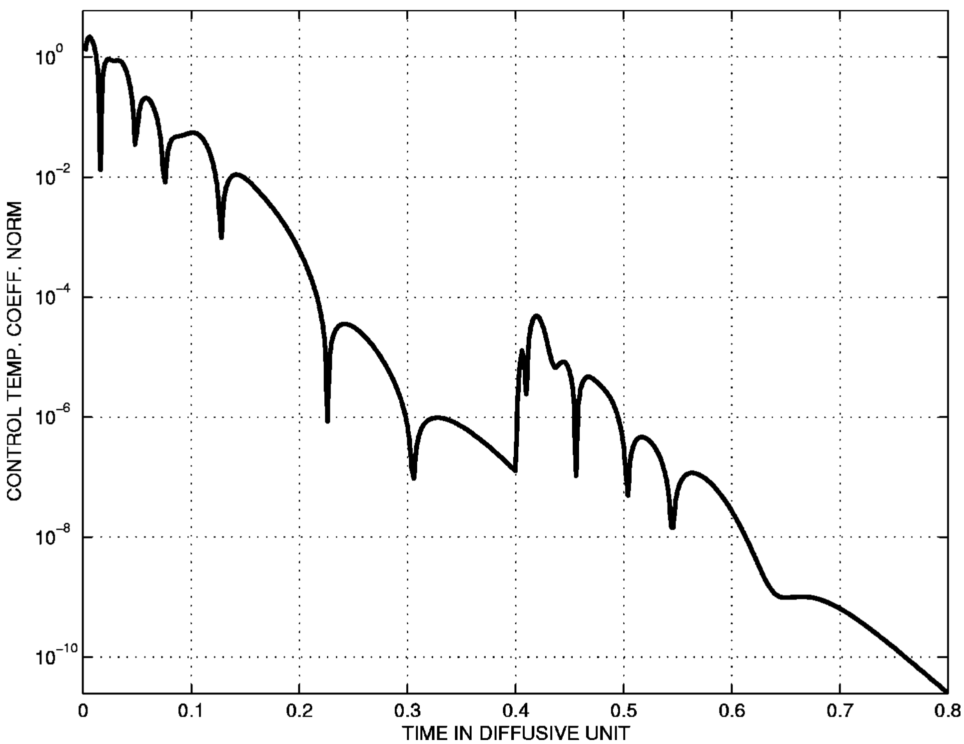

FIG. 5. Norm of closed-loop control temperature coefficients.

Ra step is accompanied by a large transient conductive temperature, but does not cause a significant transient response in the convective fields. As long as the residual convection prior to the step jump of Ra remains small, the destabilizing effects of the transient conductive temperature is insignificant. In this study the two-step Ra gain table used for demonstration purpose. A more refined, multistep gain table may be necessary for laboratory implementations. In conclusion, to suppress a fully nonlinear convection, the gain-schedule approach is a means to achieve a performance up to the linear stability limit.

ACKNOWLEDGMENT

This research is supported by the United States Air Force (Grant No. F49620-00-1-0166).

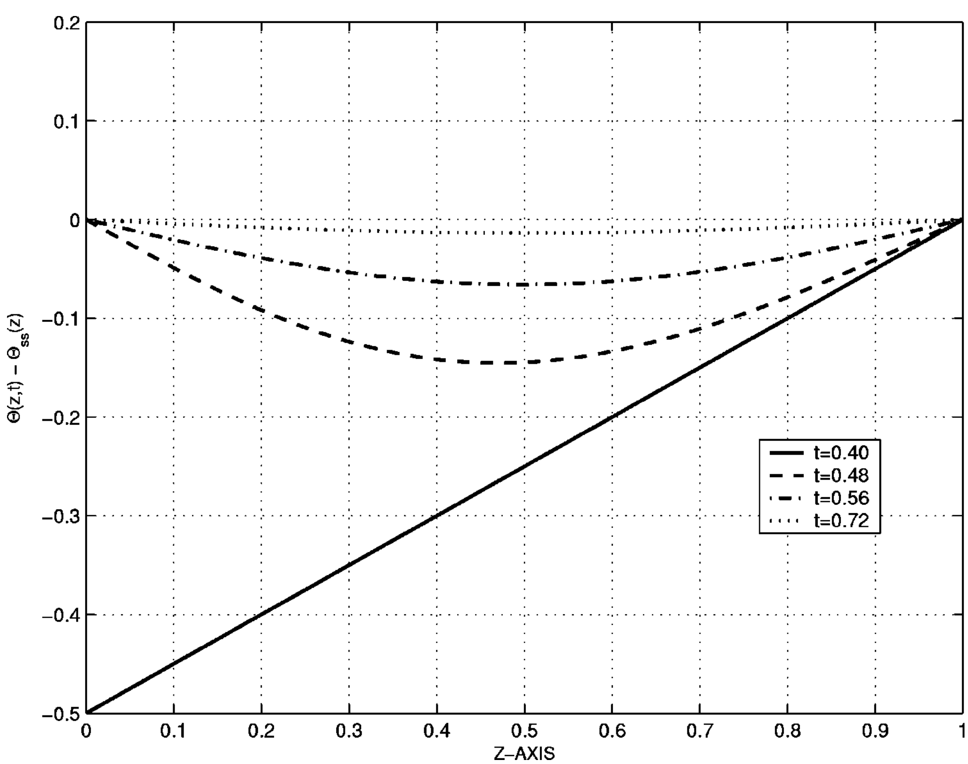

FIG. 6. Time plot of the transient conductive temperature.

APPENDIX: DERIVATION OF THE MODEL EQUATIONS

The dimensional form of the Boussinesq system consists of the momentum equation,

$$\partial_t \mathbf{v}^* + \mathbf{v}^* \cdot \nabla \mathbf{v}^* = \frac{1}{\rho} \nabla (p^* + \rho g z) - \alpha g (T_0^* - T^*)\mathbf{k} + \nu \nabla^2 \mathbf{v}^*, \tag{A1}$$

where in the buoyant force term, T_0^* is a reference temperature (at $z=0$). The heat equation is

$$\partial_t T^* + \mathbf{v}^* \cdot \nabla T^* = \kappa \nabla^2 T^*. \tag{A2}$$

The velocity field $\mathbf{v}^*=(u^*,v^*,w^*)$ satisfies the incompressibility condition

$$\nabla \cdot \mathbf{v}^* = 0. \tag{A3}$$

We use (x,y,z) and t to denote dimensional as well as nondimensional Cartesian coordinates and time for simplicity. The asterisk highlights dimensional variables. For nondimensionalization the layer thickness d and d^2/κ are used for scaling length and time; ν and κ denote the viscous and thermal diffusivity, respectively; ρ is the mean density of the fluid; α is the coefficient of thermal expansion and g is the gravitational acceleration. The upper (at $z=1$) and lower (at $z=0$) walls of the layer are prescribed, respectively, at temperatures T_2^* and T_1^* with $T_1^* > T_2^*$.

The fluid temperature, $T^*(x,y,z,t)$, is decomposed into a conductive temperature $\Theta^*(z,t)$ and a convective (perturbation) temperature $\theta(x,y,z,t)$,

$$T^*(x,y,z,t) = \Theta^*(z,t) + \theta^*(x,y,z,t). \tag{A4}$$

For most studies in RBC, a static (nominal) state is used,

$$\Theta^* = \Theta_{ss}^* = T_1^* - (T_1^* - T_2^*)z. \tag{A5}$$

For $\mathrm{Ra} > \mathrm{Ra}_c$, the steady perturbation temperature $\theta^* \neq 0$ does not vanish.

Here the full set of equations are rederived for the case when the conductive temperature is not in a steady state. The gain schedule algorithm is applied, when the Rayleigh number is increased incrementally in steps. Consider the conductive state to be static as described by Eq. (A5) at $t=t^-$. In the closed-loop response $\theta(x,y,z,t) \approx 0$ as convection is suppressed. At $t=t^+$ the lower wall temperature is increased to $T_1^* + \Delta T^*$, where $t^- \approx t^+$. The conductive temperature after the jump is given by

$$\Theta^*(z,t) = \Theta_{ss}^*(z) + \tilde{\Theta}(z,t),$$
$$\Theta_{ss}^*(z) = (T_1^* + \Delta T^*) - (T_1^* + \Delta T^* - T_2^*)z. \tag{A6}$$

The transient conductive temperature $\tilde{\Theta}(z,t)$ is governed by

$$\partial_t \tilde{\Theta}^* = \kappa \partial_{zz}^2 \tilde{\Theta}^*, \tag{A7}$$

subjected to initial and boundary conditions

$$\tilde{\Theta}^*(z,0) = -\Delta T^*(1-z), \quad \tilde{\Theta}^*(0,t) = 0, \quad \tilde{\Theta}^*(1,t) = 0. \tag{A8}$$

Next, we incorporate the decomposed temperatures into the governing equations (A1) and (A2). The conductive temperature is balanced by pressure. Equation (A1) gives

$$\partial_t \mathbf{v}^* + \mathbf{v}^* \cdot \nabla \mathbf{v}^* = -\frac{1}{\rho} \nabla (\pi^*) + \alpha g \theta^* \mathbf{k} + \nu \nabla^2 \mathbf{v}^*,$$
$$\pi^* = p^* + \rho g z + \int_0^z [\Theta^*(0,t) - \Theta^*(z',t)]dz'. \tag{A9}$$

This equation has the same form regardless of the conductive temperature. Separating the total temperature into the conductive and perturbation components, the heat equation becomes

$$\partial_t \theta^* + \mathbf{v}^* \cdot \nabla \theta^* = -w^* \partial_z \Theta^* + \kappa \nabla^2 \theta^*. \tag{A10}$$

Equations (A3), (A7), (A9), and (A10) provide the governing equations.

Introducing the nondimensional scaling, the full nondimensional governing equations of the plant model are

$$\mathrm{Pr}^{-1}(\partial_t \mathbf{v} + \mathbf{v} \cdot \nabla \mathbf{v}) = -\nabla \pi + \mathrm{Ra}\, \theta \mathbf{k} + \nabla^2 \mathbf{v}, \tag{A11}$$

$$\nabla \cdot \mathbf{v} = 0, \tag{A12}$$

$$\partial_t \theta + \mathbf{v} \cdot \nabla \theta = w(1 - \partial_z \tilde{\Theta}) + \nabla^2 \theta, \tag{A13}$$

$$\partial_t \tilde{\Theta} = \partial_{zz}^2 \tilde{\Theta}. \tag{A14}$$

In the gain schedule approach, the step increase in Ra imparts a discontinuity in the thermal field of the system. This condition translates an initial condition for the conductive temperature at $t=t^+$,

$$\tilde{\Theta}(z,t^+) = -\frac{\Delta T^*(1-z)}{(T_1^* + \Delta T^* - T_2^*)}. \tag{A15}$$

Thus a transient response follows each jump $\tilde{\Theta}$ where $\tilde{\Theta} \to 0$ as the conductive temperature approaches steady state.

[1] A. E. Bryson and Y. C. Ho, *Applied Optimal Control* (Hemisphere, New York, 1975).
[2] M. C. Cross and P. C. Hohenberg, Rev. Mod. Phys. **65**, 851 (1993).
[3] J. Tang and H. H. Bau, Proc. R. Soc. London, Ser. A **447**, 587 (1994).
[4] L. E. Howle, Phys. Fluids **9**, 3111 (1997).
[5] L. E. Howle, Int. J. Heat Mass Transfer **40**, 817 (1997).
[6] L. E. Howle, Phys. Fluids **9**, 1861 (1997).
[7] J. Tang and H. H. Bau, J. Fluid Mech. **363**, 153 (1998).
[8] J. Tang and H. H. Bau, Phys. Fluids **10**, 1597 (1998).
[9] A. C. Or, L. Cortelezzi, and J. L. Speyer, J. Fluid Mech. **437**, 175 (2001).
[10] A. C. Or and J. L. Speyer, J. Fluid Mech. **483**, 111 (2003).
[11] L. E. Howle, J. Fluid Mech. **411**, 39 (2000).
[12] L. Cortelezzi and J. L. Speyer, Phys. Rev. E **58**, 1906 (1998).